

Structure and kinetics in the freezing of nearly hard spheres

Jade Taffs and C. Patrick Royall

School of Chemistry, University of Bristol, Bristol, BS8 1TS, UK.

Stephen R. Williams

Research School of Chemistry, Australian National University, Canberra, ACT 0200, Australia.

Hajime Tanaka

*Institute of industrial science, The University of Tokyo,
4-6-1 Komaba, Meguro-ku, Tokyo, 153-8505, Japan.*

We consider homogeneous crystallisation rates in confocal microscopy experiments on colloidal nearly hard spheres at the single particle level. These we compare with Brownian dynamics simulations by carefully modelling the softness in the interactions with a Yukawa potential, which takes account of the electrostatic charges present in the experimental system. Both structure and dynamics of the colloidal fluid are very well matched between experiment and simulation, so we have confidence that the system simulated is close to that in the experiment. In the regimes we can access, we find reasonable agreement in crystallisation rates between experiment and simulations, noting that the larger system size in experiments enables the formation of critical nuclei and hence crystallisation at lower supersaturations than the simulations. We further examine the structure of the metastable fluid with a novel structural analysis, the topological cluster classification. We find that at densities where the hard sphere fluid becomes metastable, the dominant structure is a cluster of $m = 10$ particles with five-fold symmetry. At a particle level, we find three regimes for the crystallisation process: metastable fluid (dominated by $m = 10$ clusters), crystal and a transition region of frequent hopping between crystal-like environments and other ($m \neq 10$) structures.

I. INTRODUCTION

Crystallisation is a long-standing challenge, due not least to its local nature, where rare events on microscopic time- and length-scales initiate the phase transition [1]. This lack of understanding of crystallisation can have very significant practical consequences, for example in control of drug production [2]. It appears challenging to make much progress with conventional materials, due to the local nature of nucleation events which lead to crystallisation, however particle-resolved studies of model systems such as colloidal dispersions which capture the essential thermodynamics provide the necessary

detail required [3].

Colloidal ‘hard’ spheres are important in the understanding of crystallisation. Few systems have received so much attention, not least because both simulations and experiments can access relevant timescales and particle-level structural lengthscales [4–8]. The general phenomenology of hard sphere crystallisation has been well established for a decade [9]: at low supersaturations, close to the hard sphere freezing transition at a volume fraction of $\phi_f = 0.494$ [10], crystallisation is dominated by rare events leading to the formation of large nuclei. Higher supersaturation leads to a very strong rise in nucleation rate, and upon increasing the volume fraction, approaching the hard sphere glass transition, crystallisation has been observed at times less than the structural relaxation time [11, 12], while at higher volume fractions still ($\phi = 0.62$), crystallisation is not seen on the experimental timescale. Despite this phenomenology, very large discrepancies have been found in nucleation rates predicted by simulation using biased ensemble averaging and experiment [4, 5, 13], which remain unexplained [14, 15]. Neither the inclusion of polydispersity [5, 13] nor electrostatic charge [16] in the simulations has resolved this situation, although the former has been shown to have profound and complex consequences for nucleation [17, 18].

Charles Frank originally suggested that 13-membered icosahedra might suppress crystallisation in the Lennard-Jones system [19], and recently there has been a resurgence of interest in the role of local structure in crystallisation. In simulations of hard spheres, five-fold symmetry has been identified both with the suppression of

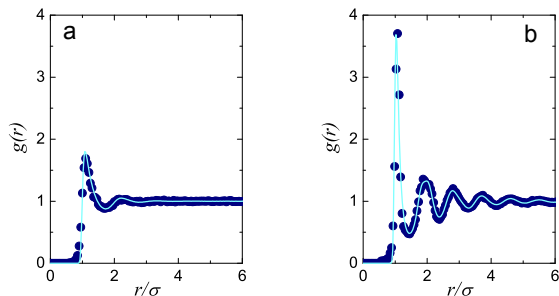


FIG. 1: (color online) Radial distribution functions in experiment and simulation. (a) low density, $\phi = 0.27$, (b) higher density $\phi = 0.53$. In both cases, simulation parameters were carefully adjusted to experiment. Line, simulation data, circles, experimental data.

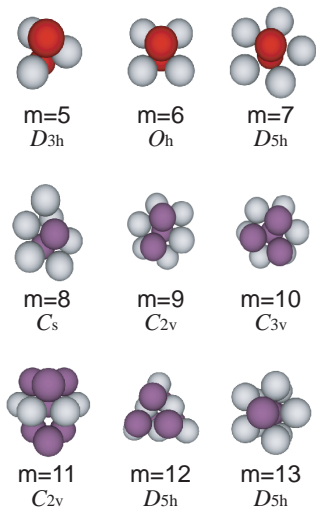


FIG. 2: (color online) Clusters detected by the topological cluster classification. These structures are minimum energy clusters of the Morse potential with $\rho_0 = 25.0$ [36].

crystallisation [20, 21] and found at the centre of crystal nuclei [22]. Locally dense amorphous crystal precursors have been identified in the metastable hard sphere fluid [23] and have also been found in softened systems [24, 25]. One of us identified a mechanism for crystallisation through increased crystal-like ordering in the fluid prior to the formation of a nucleus, thereby lowering the free energy barrier [26–28], and that this entails no change in local density [29]. It was also shown that in weakly size-asymmetric binary hard sphere systems, crystallites can form quickly, but apparently become ‘poisoned’ [30].

Pioneering particle-resolved experiments [6] identified local structure, and more recent experiments on ‘hard’ spheres too polydisperse to crystallise have shown a degree of fivefold symmetry which, along with local crystalline order, has been related to slow dynamics [31]. Here we consider local structure in crystallisation in a particle-resolved colloidal model system. While such experimental studies can in principle resolve mechanisms of crystallisation, quantitative comparison to simulation and theory is very challenging, due to the limited accuracy with which colloidal volume fractions can be measured [32], combined with the lack of control over (and often knowledge of) interparticle interactions upon which crystallisation rates critically depend [16, 33, 34]. Quantitative agreement between experiment and simulation has been obtained in the case of *heterogeneous* crystallisation of nearly hard spheres, initiated by a wall, where the crystallisation rate is less sensitive to the volume fraction compared to homogenous crystallisation [35].

Here we present a careful comparison of experiment and simulation in a system of nearly hard spheres which undergo homogenous nucleation. We interpret our results with a novel structural method, the topological clus-

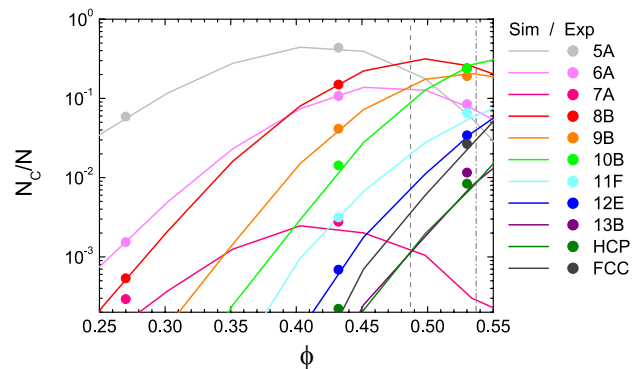


FIG. 3: (color online) Structural changes upon increasing density in the nearly-hard sphere fluid. Lines are simulation, according to eq. 1, circles are experiment. Data for metastable fluids (some of which subsequently crystallise) are taken at times $\ll \tau_x$. Dashed lines are estimated freezing and melting volume fractions for our system, as described in section II B. [40].

ter classification (TCC) [37–39], which directly identifies a number of local structures. Our mapping between experiment and simulation reveals good agreement in crystallisation rates at the range of supersaturation we accessed. We find that the metastable fluid is dominated by 10-membered fivefold symmetric structures reminiscent of the 13-membered icosahedra proposed long ago as a mechanism for the suppression of crystallisation [19].

II. METHODS

A. Experimental

We used polymethyl methacrylate (PMMA) particles of diameter $2.00 \mu\text{m}$ with a polydispersity of 4.0 % as determined by static light scattering. This degree of polydispersity is insufficient to have much impact on phase behaviour [41]. Swelling of the colloids cannot be ruled out in the density and refractive index matching solvent mixture of cis-decalin and cyclohexyl bromide used [32]. However, as far as crystallisation is concerned, electrostatic charge, which is not entirely screened by the tetrabutyl ammonium salt added contributes a further degree of uncertainty in determining the effective colloid volume fraction. If ignored, the effects of electrostatics are quite sufficient to leave measures of crystallisation rates quantitatively meaningless [16, 34]. For this reason we map simulations carefully to the experiments. We use confocal microscopy (Leica SP5) to track the particle coordinates. Heterogenous nucleation is prevented by weakly sintering larger ($3.5 \mu\text{m}$) polydisperse colloids onto the wall of the sample cell. We imaged at least $50 \mu\text{m}$ from the wall and saw no sign of heterogeneous crystallisation.

B. Mapping simulation to experiment

Crystallisation experiments are compared with standard Brownian dynamics (BD) simulations, with a system size of $N = 2048$ and 10976 particles and a timestep of 0.1 simulation time units. Fitting of the experimental radial distribution function is carried out using Monte Carlo (MC) simulations with $N = 2048$ particles. Both the BD and MC simulations are carried out in the canonical (NVT) ensemble. Our particle-resolved experiments enable an innovation: simulations take as their starting point experimental coordinates sampled from a fluid at a time small compared to that required for crystallisation. These are treated with 160 MC sweeps to remove small overlaps resulting from coordinate tracking errors. Particle interactions are modelled with a truncated Morse potential with a Yukawa component, which approximate the hard core and electrostatic charging of the colloidal particles respectively.

$$\beta u(r) = \beta \varepsilon_{TM} \left[1 + e^{\rho_0(1-r/\sigma_{ij})} \left(e^{\rho_0(1-r/\sigma_{ij})} - 2 \right) \right] + \beta \varepsilon_Y \frac{e^{-\kappa(r/\sigma_{ij}-1)}}{r/\sigma_{ij}} \quad (1)$$

Here the shifted Morse component (left term) is truncated at $r = \sigma_{ij}$ (where it vanishes) and the Yukawa component (right term) is truncated at $r = 2\sigma_{ij}$. $\beta = 1/k_B T$ the thermal energy, σ_{ij} is the mean of the diameters of colloids i and j and r is the center separation. The truncated Morse potential is fixed with strength $\varepsilon_M = 1.0$ and range parameter $\rho_0 = 25.0$. The contact potential of the Yukawa contribution $\beta \varepsilon_Y = Z^2 \lambda_B / [(1 + \kappa\sigma/2)^2 \sigma]$. Here Z is the number of charges on the colloid and λ_B is the Bjerrum length. The inverse Debye screening length is denoted by $\kappa = \sqrt{4\pi\lambda_B\rho_{ion}}$ where ρ_{ion} is the number density of (monovalent) ions.

We fix the Yukawa parameters to the experimental data. Our approach follows [42, 43], where the Yukawa interaction parameters $\beta \varepsilon_Y$ and $\kappa\sigma$ are adjusted such that the experimental radial distribution function is well reproduced by the simulation (Fig. 1). In this case we find $\kappa\sigma = 30.0 \pm 5.0$ and $\beta \varepsilon_Y = 1.0 \pm 0.25$, which corresponds to a Debye length of 67 nm (or an ionic strength of 1.4 μM) and colloid charge of $Z = 200$. These are comparable to previous work on similar systems [42–46].

We treat polydispersity with a Gaussian distribution in σ with 4% standard deviation (the same value as the size polydispersity in the experimental system). The radial distribution function of each experimental state point was fitted for a (metastable) fluid with MC simulation. We then quote the state point in units of $\phi = V_{part}/V_{box}$ where the volume of the particles is taken as $V_{part} = \frac{\pi}{6} \sum_i \sigma_i^3$.

There are a variety of ways to estimate the freezing transition for a system of weakly repulsive spheres. Among the more accurate [34] appears to be to interpolate exact simulation results for hard-core Yukawa

systems [40] with the hard sphere values. This yields volume fractions for freezing and melting for a weakly charged system. Since we use a slightly softened core here, we estimate the impact of this softening on the phase behaviour by calculating the Barker-Henderson effective hard sphere diameter σ_{eff}

$$\sigma_{eff} = \int_0^\infty dr [1 - \exp(-\beta u(r))], \quad (2)$$

where $u(r)$ is the interaction potential, i.e. Eq. (1) or a hard core with the same Yukawa term. The effective hard sphere diameters are $\sigma_{eff}^{HCYUK} = 1.021\sigma$ and $\sigma_{eff}^{TMYUK} = 1.018\sigma$ for the hard-core Yukawa and the truncated Morse system we use here. To approximately include the slight effect of the core softening, we scale the volume fractions for freezing and melting by $(\sigma_{eff}^{HCYUK}/\sigma_{eff}^{TMYUK})^3$. The core softening then leads to a change of around 0.004 in ϕ in addition to the effect of the Yukawa repulsion. Thus for our system, we estimate the freezing volume fraction $\phi_f = 0.487$ and melting $\phi_m = 0.537$. Note that we neglect the effect of the 4% polydispersity, whose impact on the freezing and melting volume fractions we expect to be slight [41].

C. Structural Analysis - Topological Cluster Classification

To analyse the structure, we identify the bond network using a maximum bond length of 1.4σ and a modified Voronoi construction [37]. For bond lengths greater than 1.4σ , the network in condensed systems is insensitive to the bond length. Having identified the bond network, we use the Topological Cluster Classification (TCC) to determine the nature of the local environment of each particle [37, 39]. This analysis identifies all the shortest path three, four and five membered rings in the bond network. We use the TCC to find structures topologically identical to clusters which are global energy minima of the Morse potential for the range we consider $\rho_0 = 25.0$, as listed in [36] and illustrated in Fig. 2.

Now the system we consider interacts not via a full Morse potential, rather our truncation takes the repulsive component only, in a similar spirit to the approach Weeks, Chandler and Andersen (WCA) used for the Lennard-Jones model [47]. While that approach is well-known to reproduce accurately the fluid structure at the pair level, one might expect deviations for higher-order structure such as that probed by the TCC. In fact we found that for short-ranged systems, clustering is *enhanced* in the case of truncation [48]. Unlike many analyses, for example those which use bond-orientational order parameters [49], our emphasis on bond topology distinguishes between icosahedra and the 13 -membered D_{5h} structure illustrated in Fig. 2 which is the minimum energy cluster for the Morse potential with $(\rho_0 = 25.0)$.

We have also checked for the icosahedron and found small quantities ($\lesssim 1\%$) [48]. In addition we identify the thirteen particle structures which correspond to FCC and HCP in terms of a central particle and its twelve nearest neighbours. For more details see [37, 39]. If a particle is a member of more than one cluster, we take it to reside in the larger cluster.

III. RESULTS

A. Fluid structure: matching state point

We begin our presentation of results by considering the stable and metastable fluids. For metastable fluids, the cluster populations are sampled from the period prior to crystallisation (see next section). The topological cluster classification (TCC) analysis shows a considerable increase in cluster populations as a function of volume fraction, as shown in Fig. 3. Some smaller clusters are subsumed into larger clusters for $\phi \gtrsim 0.55$. We see a sharp rise in the fivefold symmetric 10-membered C_{2v} cluster we term ‘10B’ following [36], such that by $\phi \gtrsim 0.54$, it is the dominant cluster in the fluid. We estimate freezing in our nearly hard sphere system at $\phi = 0.487$ as noted in section II C. We note that the experimental and simulation data are very well-matched in Fig. 3. This gives us confidence that the fluid structure of the experiments is accurately reproduced in simulation, in other words that the state point is well matched and that we are therefore in a strong position to investigate any possible discrepancies between the experimental and simulated system.

B. Matching timescales

The timescales in the experiments and simulations are matched as follows. The dynamics slow upon increasing ϕ and we define a structural relaxation time from the intermediate scattering function (ISF). We determine the intermediate scattering function (ISF) $F(\mathbf{k}, t) = \langle \cos(\mathbf{k} \cdot (\mathbf{r}(t+t') - \mathbf{r}(t'))) \rangle$ where the wavevector \mathbf{k} is taken close to the main peak in the static structure factor and \mathbf{r} is the location of each particle at time t and the angle brackets denote a statistical average. An ISF is shown in Fig. 4. We fit the tail of the ISF with a stretched exponential $F(\mathbf{k}, t) = C \exp[-(t/\tau_\alpha)^\beta]$ to obtain the structural relaxation time τ_α . We obtain $C = 0.99$, $\tau_\alpha = 30.5$ s, $\beta = 0.8134$. τ_α is then plotted as a function of ϕ in Fig. 5. The data are well described by a Vogel-Fulcher-Tammann (VFT) relation $\tau_\alpha = \tau_0 \exp[D\phi/(\phi_0 - \phi)]$ where τ_0 is a relaxation time in the normal liquid, D is the ‘fragility index’, and $\phi_0 \approx 0.616$ is the ideal glass transition volume fraction [28]. We assume the scaling of the dynamics at this volume fraction is the same for experiment and simulation. We equate the experimental and simulation structural relaxation times at $\phi = 0.43$.

Thus both experiment and simulation τ_α are taken from the VFT fit (Fig. 5).

C. Structure in crystallisation

The process of crystallisation is shown in Fig. 6. Here $\phi = 0.54$. Note that some small crystalline regions are present at $t = 0$. We have previously demonstrated that even stable fluids have populations of particles in crystalline environments [48], as shown in Fig. 3, this rises markedly around the freezing transition. These images suggest that the metastable fluid shows relatively little change for $27.9\tau_\alpha \leq t$, but crystallisation subsequently occurs at $27.9\tau_\alpha \leq \tau_x \leq 316.9\tau_\alpha$. Henceforth we define τ_x as the time at which 40% of the particles are identified in crystalline environments. Moderate changes to this threshold have no impact upon our conclusions.

We now turn to a TCC analysis of the crystallisation process. Figure 7 shows the population in each TCC cluster as a function of time for experiment (a) and simulation (b). In both experiment and simulation, we identify three regimes. For $t \lesssim 10\tau_\alpha$ in the experiment and $t \lesssim 40\tau_\alpha$ in the simulation there is little change in cluster populations. At intermediate times approaching τ_x (here $\tau_x = 107$ and $64\tau_\alpha$ for this experiment and simulation run respectively), we see a steady growth in particles identified in crystalline environments (predominantly FCC) at the expense of particles in fluid environments. Most notable of the non-crystalline clusters is 10B, which drops continuously throughout this period. At the level of this description, then, crystallisation is interpreted as the conversion of 10B clusters into FCC environments. At times larger than τ_x , there is a further decrease in non-crystalline clusters. However, note that, on the timescale of these experiments and simulations, a reasonable population (a few percent) of non-crystalline clusters remain at all times.

D. Comparison between experiment and simulation

We now compare crystallisation times in simulation and experiment. Recall that nucleation of ‘hard’ spheres is found to exhibit strong deviations between experiment and simulation [4, 14]. We compare crystallisation times as shown in Fig. 8. We see a reasonable agreement for moderate values of $\phi \gtrsim 0.56$, but at lower supersaturation $\phi \lesssim 0.55$ or $\phi - \phi_M \lesssim 0.01$, we find an emergent discrepancy between experiment and simulation. While no mapping between experiment and simulation is perfect [32, 34], our careful analysis of state point and timescale leads us to believe that this discrepancy is not accounted for by a shift of ϕ .

Now neither the simulations we employ here, *nor the confocal microscopy experiments* access the regime of low supersaturation where the formation of a large nucleus is

a rare event. In simulation, biasing techniques can be employed, and while similar methodologies are in principle possible in experiment [50] the kind of precision required to determine nucleation rates quantitatively remains some way off. An important point then, is that unbiased simulation and confocal microscopy experiment access similar regimes of supersaturation. However the experiment has a rather larger system size than does the simulation. The simulation box size is typically 2000 and 10,000 σ^3 for the $N = 2048$ and 10976 system sizes respectively, while the experiments are confined in capillaries of size $250\sigma \times 250\sigma \times 2500\sigma \sim 1.6 \times 10^8 \sigma^3$. The imaging volume ($50\sigma \times 50\sigma \times 25\sigma \sim 6.3 \times 10^5 \sigma^3$) is rather smaller than the whole system and crystals can nucleate outside this region (Fig. 6). The rate of crystal growth has recently been determined in a very similar system [35], and the associated timescales are of order $100\text{--}1000\tau_\alpha$, suggesting that for long times, crystals can spread throughout the sample, so the relevant volume is that of the entire system, rather than just the imaging volume. Thus, decreasing the supersaturation to $\phi - \phi_M \approx 0.005$, we see that experiments continue to crystallise, but for simulations, the time for crystallisation moves outside the accessible timescale. Note that, at higher supersaturation, nucleation rates increase strongly, so the crystallisation time τ_x is somewhat independent of system size.

While the argument presented above is physically attractive, we seek a more quantitative validation, and for this we turn to the results of Filion *et al.* [14]. Clearly, for the system to crystallise, at least one nucleation event must occur. Taking the nucleation rate for the highest volume fraction in ref. [14], for a monodisperse system $J = 1.4 \times 10^{-5} \sigma^3 \tau_B$ where τ_B is the time to diffuse a diameter in the dilute limit and is equal to $0.63\tau_\alpha$ ($\phi = 0.43$). The corresponding volume fraction relative to melting is $\phi - \phi_M = 0.0051$. For our system, this corresponds to one nucleation event every 4.0 and 21.6 τ_α ($\phi = 0.43$) for $N = 10976$ and $N = 2048$ respectively. In other words, in our simulation timescales, we expect crystallisation.

However, the rate of nucleation is highly sensitive to *polydispersity* [5, 13], which is 4% here. Recall this is expected to have little effect on the equilibrium phase diagram [41]. While to the best of our knowledge, no precise predictions for nucleation rates in polydisperse systems have been made for the regime we access ($\phi \gtrsim \phi_M$), it seems reasonable to expect a shift of the nucleation rate as a function of ϕ by ~ 0.015 which has been found at lower supersaturation [5, 13]. We note that the shape of the particle size distribution, rather than just its second moment, can be important [17, 18], however here we shall assume that the effect of polydispersity is to effect a shift in ϕ of 0.015 in the nucleation rate. In other words, we take the rate for $\phi - \phi_M = -0.01$ for a monodisperse system to apply for $\phi - \phi_M = 0.005$ for our system. The nucleation rate at $\phi - \phi_M = -0.01$ is four orders of magnitude lower than that at $\phi - \phi_M = 0.005$ [14]. At such low rates, we expect no nucleation in simulation, but the

larger system size in experiment (concoincidentally four orders of magnitude larger than the simulation) is sufficient for nucleation to occur on our timescales, as is consistent with the crystallisation that we see.

If this analysis is correct, for a monodisperse system at $\phi - \phi_M = 0.005$ we should expect a much higher nucleation rate, and crystallisation on the simulation timescale. To verify this point, we carried out some simulations with a monodisperse system. These are shown in Figs. 8(a and b), and indeed crystallise in the regime of interest. We thus conclude that, in the regime we access, the discrepancy between experiment and simulation is likely due to the larger system size in the case of the experiments.

E. Particle-level crystallisation mechanism

Our single-particle analysis gives us the ability to shed some light on the mechanism of crystallisation. We have noted that the metastable fluid is dominated by the five-fold symmetric 10B cluster. In Fig. 9, we show the history of a single particle, throughout a simulation for $\phi = 0.55$ and $\phi = 0.58$. We see that each particle fluctuates and is identified in a number of different structures, including local crystalline environments. Three regimes emerge: the metastable fluid, dominated by the 10B cluster, the final crystal, and a transition regime between the two. Note that in the transition regime, although the particle is often found in amorphous structures, these are rarely 10B. This suggests that 10B-crystal transitions may be somehow suppressed. This is consistent with long-standing ideas that five-fold symmetry can suppress crystallisation [19] and very recent experimental [31] work which suggests frustration between five-fold symmetry and local crystalline order. We would thus expect that 10B clusters are rather stable (see below). During growth, however, it is possible that a crystalline surface may disrupt the five-fold symmetry in the fluid, leading to more rapid transformation between 10B and crystalline structures. Our finding of a transition regime further supports findings that crystallisation preferentially takes place in a region of high crystal-like bond orientational order [26, 28, 29].

We close by considering the stability of the fivefold symmetric 10B cluster. This seems to dominate the metastable fluid at densities where crystallisation occurs. In Fig. 10 we show transition probabilities from the 10B cluster to various geometries. We see there is a tendency to remain in the 10B cluster. That is, the 10B cluster shows a higher degree of stability than other clusters. In other words, for the nearly hard sphere fluid, the 10B is a locally preferred structure, similar to icosahedra and related polyhedra in glass-forming systems [49, 51–55]. This is consistent with previous reports that five-fold symmetry is favoured in ‘hard’ spheres [20, 21, 31]. The fact that this ordering tendency to structures of five-fold character such as 10B appears to be enhanced at higher

ϕ is intriguing, as at higher volume fractions still, ‘spinodal’ crystallisation takes place in a small fraction of τ_α as found previously [11, 12]. In such unstable fluids, however, we cannot measure the lifetime of 10B clusters: the stability of 10B is exceeded by the thermodynamic driving force of crystal nucleation.

IV. CONCLUSION

We have carefully matched simulation to experiment for a nearly hard sphere system. For the regimes in which we can access crystallisation, the kinetics are similar in both simulation and experiment with the exception that, at lower volume fraction, experiments crystallise faster than simulations. We believe these are associated with the onset of low nucleation rates as the supersaturation is decreased. Under these conditions, the larger experimental system size means nucleation events occur on accessible timescales, enabling crystallisation to be observed in experiments but not in simulations. While accurate simulation data has been obtained for monodisperse systems across a wide range of ϕ , the effect of polydispersity characteristic of colloidal experiments has only been considered for nucleation rates too low for confocal microscopy experiments to access. In order to be confident that no discrepancy exists, predictions for polydisperse systems in the regime accessible to experiments such as ours would be helpful.

Our topological cluster classification reveals the mechanism of crystallisation. In particular, around the freezing transition, nearly hard sphere fluids become dominated by a five-fold symmetric ten-membered cluster which we term 10B. By considering particle histories, we find that transitions between this 10B cluster and crystalline environments are suppressed. Instead, after some time in a metastable fluid state, with occasional excursions

to a crystalline environment, which usually occur through an intermediate structure, the particle finds itself in a transition state, presumably due to the proximity of a crystalline region which stabilises local crystalline environments. In the transition state, the particle spends large amounts of time in a crystalline environment, and almost no time in a 10B cluster, instead it is found in other amorphous clusters. Eventually, the particle spends all its time in a local crystalline environment and is said to be crystalline. The transition regime we observe may be related to the ‘cloud’ identified in the case of softened particles [24].

Finally, we emphasise that, since absolutely hard spheres are not found in nature [34], it is essential to take account of the inherent softness in any experimental system. However, comparison with true hard spheres suggests that the main effect of the softness we have considered is to shift the state point such that we must consider effective volume fractions. This is consistent with previous observations that mapping the effective packing fraction to hard spheres results in a practically identical fluid structure [48].

Acknowledgements

It is a pleasure to thank Kurt Binder, Bob Evans, Daan Frenkel, Rob Jack, Mathieu Leocmach, Thomas Palberg, John Russo, Richard Sear, and Frank Schrieber for stimulating discussions and Monica Moreno for preliminary simulations and experiments. CPR gratefully acknowledges the Royal Society for financial support and EPSRC grant code EP/H022333/1 H.T. acknowledges a grant-in-aid from the Ministry of Education, Culture, Sports, Science and Technology, Japan and Aihara Project, the FIRST program from JSPS, initiated by CSTP.

-
- [1] R. P. Sear, *J. Phys.: Condens. Matter* **19**, 033101 (2007).
 - [2] S. L. Morissette, *Proc. Nat. Acad. Sci.* **100**, 2180 (2003).
 - [3] A. Ivlev, H. Loewen, G. E. Morfill, and R. C. P., *Complex Plasmas and Colloidal Dispersions: Particle-resolved Studies of Classical Liquids and Solids* (World Scientific, 2012).
 - [4] S. Auer and D. Frenkel, *Nature* **409**, 1020 (2001).
 - [5] S. Auer and D. Frenkel, *Nature* **413**, 711 (2001).
 - [6] U. Gasser, E. R. Weeks, A. Schofield, P. N. Pusey, and D. A. Weitz, *Science* **292**, 258 (2001).
 - [7] D. W. Aastuen, N. A. Clark, L. K. Cotter, and B. J. Ackerson, *Phys. Rev. Lett.* **57**, 1733 (1986).
 - [8] J. L. Harland and W. van Megen, *Phys. Rev. E* **55**, 3054 (1997).
 - [9] T. Palberg, *J. Phys.: Condens. Matter* **11**, R323 (1999).
 - [10] W. G. Hoover and F. Ree, *J. Chem. Phys.* **49**, 3609 (1968).
 - [11] E. Zaccarelli, C. Valeriani, E. Sanz, W. C. K. Poon, M. E. Cates, and P. N. Pusey, *Phys. Rev. Lett.* **103**, 135704 (2009).
 - [12] E. Sanz, C. Valeriani, W. C. K. Zaccarelli, E. Poon, P. N. Pusey, and M. E. Cates, *Phys. Rev. Lett.* **106**, 215701 (2011).
 - [13] S. Auer and D. Frenkel, *Ann. Rev. Phys. Chem.* **55**, 333 (2004).
 - [14] L. Filion, R. Ni, D. Frenkel, and M. Dijkstra, *J. Chem. Phys.* **134**, 134901 (2011).
 - [15] T. Schilling, S. Dorosz, H. J. Schoepe, and G. Opletal, *J. Phys.: Condens. Matter* **23**, 194120 (2011).
 - [16] S. Auer and D. Frenkel, *J. Phys.: Condens. Matter* **14**, 7667 (2002).
 - [17] H. J. Schoepe, G. Bryant, and W. van Megen, *Phys. Rev. Lett.* **96**, 175701 (2006).
 - [18] H. Schoepe, G. Bryant, and W. van Megen, *The Journal of Chemical Physics* **127**, 084505 (2007).
 - [19] F. C. Frank, *Proc. R. Soc. Lond. A* **215**, 43 (1952).
 - [20] N. C. Karayiannis, R. Malshe, J. J. de Pablo, and M. Laso, *Phys. Rev. E* **83**, 061505 (2011).

- [21] N. Karayiannis, R. Malshe, M. Kröger, J. J. de Pablo, and M. Laso, *Soft Matter* **8**, 844 (2012).
- [22] B. O'Malley and I. Snook, *Phys. Rev. Lett.* **90**, 085702 (2003).
- [23] T. Schilling, H. J. Schoepe, M. Oettel, G. Opletal, and I. Snook, *Phys. Rev. Lett.* **xx**, xx (2010).
- [24] W. Lechner, C. Dellago, and P. G. Bolhuis, *Phys. Rev. Lett.* **106**, 085701 (2011).
- [25] J. Russo and H. Tanaka, *Soft Matter* **8**, 4206 (2012).
- [26] T. Kawasaki and H. Tanaka, *Proc. Nat. Acad. Sci.* **107**, 14036 (2010).
- [27] T. Kawasaki and H. Tanaka, *Proc. Nat. Acad. Sci. USA* **108**, 156335 (2011).
- [28] K. Kawasaki and H. Tanaka, *J. Phys: Condens. Matter* **22**, 232102 (2010).
- [29] J. Russo and H. Tanaka, *ArXiv* p. 1109.0107 (2011).
- [30] S. R. Williams, C. P. Royall, and G. Bryant, *Phys. Rev. Lett.* **100**, 225502 (2008).
- [31] M. Leocmach and H. Tanaka, submitted (2012).
- [32] W. C. K. Poon, E. R. Weeks, and C. P. Royall, *Soft Matter* **8**, 21 (2012).
- [33] S. Auer, W. C.-K. Poon, and F. D., *Phys. Rev. E* **67**, 020401(R) (2003).
- [34] C. P. Royall, W. C. K. Poon, and E. R. Weeks, *ArXiv* p. 1205.6665 (2012).
- [35] K. Sandomirski, H. Allahyarov, E. Loewen, and S. U. Egelhaaf, *Soft Matter* **7**, 8050 (2011).
- [36] J. P. K. Doye, D. J. Wales, and R. S. Berry, *J. Chem. Phys.* **103**, 4234 (1995).
- [37] S. R. Williams, *Cond. Mat. ArXiv* **ArXiv:0705.0203v1** (2007).
- [38] C. P. Royall, S. R. Williams, T. Ohtsuka, and H. Tanaka, *Nature Mater.* **7**, 556 (2008).
- [39] A. Malins, J. Eggers, and C. P. Royall, Submitted (2012).
- [40] A. P. Hynninen and M. Dijkstra, *Phys. Rev. E* **68**, 021407 (2003).
- [41] P. Sollich and N. B. Wilding, *Phys. Rev. Lett.* **104**, 118302 (2010).
- [42] C. P. Royall, M. E. Leunissen, and A. van Blaaderen, *J. Phys.: Condens. Matter* **15**, S3581 (2003).
- [43] C. P. Royall, M. E. Leunissen, A.-P. Hynninen, M. Dijkstra, and A. van Blaaderen, *J. Chem. Phys.* **124**, 244706 (2006).
- [44] A. Yetiraj and A. van Blaaderen, *Nature* **421**, 513 (2003).
- [45] C. P. Royall, A. A. Louis, and H. Tanaka, *J. Chem. Phys.* **127**, 044507 (pages 8) (2007).
- [46] A. I. Campbell, V. J. Anderson, J. S. van Duijneveldt, and P. Bartlett, *Phys. Rev. Lett.* **94**, 208301 (2005).
- [47] J. D. Weeks, D. Chandler, and H. C. Andersen, *J. Chem. Phys.* **54**, 5237 (1971).
- [48] J. Taffs, A. Malins, S. R. Williams, and C. P. Royall, *J. Chem. Phys.* **133**, 244901 (2010).
- [49] P. J. Steinhardt, D. R. Nelson, and M. Ronchetti, *Phys. Rev. B* **28**, 784 (1983).
- [50] M. Hermes, E. C. M. Vermolen, M. E. Leunissen, D. L. J. Vossen, P. D. J. van Oostrum, M. Dijkstram, and A. van Blaaderen, *Soft Matter* **7**, 4623 (2011).
- [51] H. Jonsson and H. C. Andersen, *Phys. Rev. Lett.* **60**, 2295 (1988).
- [52] T. Tomida and T. Egami, *Phys. Rev. B* **52**, 3290 (1995).
- [53] M. Dzugutov, S. I. Simdyankin, and F. H. M. Zetterling, *Phys. Rev. Lett.* **89**, 195701 (2002).
- [54] D. Coslovich and G. Pastore, *J. Chem. Phys.* **127**, 124504 (2007).
- [55] A. Malins, J. Eggers, C. P. Royall, S. R. Williams, and H. Tanaka, *ArXiv* p. 1203.1732 (2012).

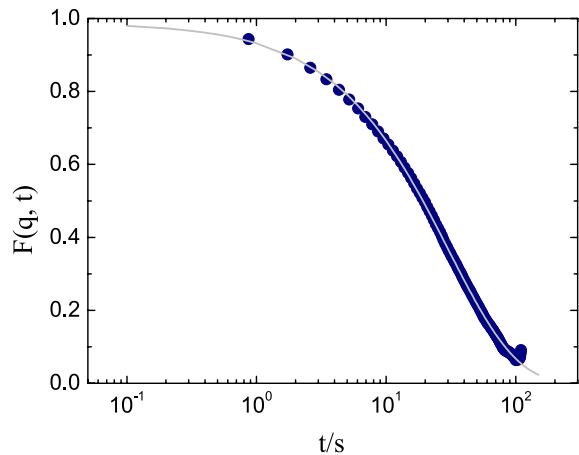


FIG. 4: Intermediate scattering function for experimental data at $\phi = 0.43$. The wavevector is taken close to the first peak in the static structure factor. Grey line is a stretched exponential fit (see text for details).

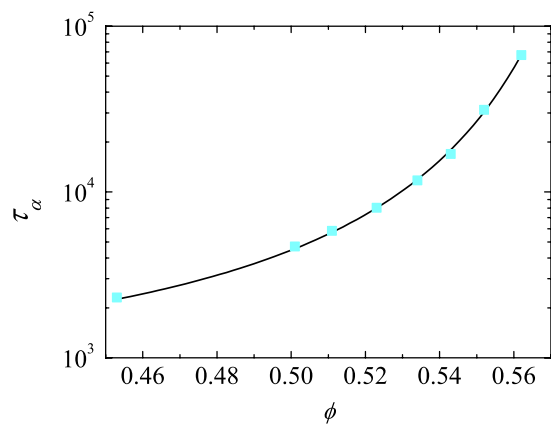


FIG. 5: (color online) Structural relaxation time as a function of ϕ . Solid line is a Vogel-Fulcher-Tammann fit (see text for details).

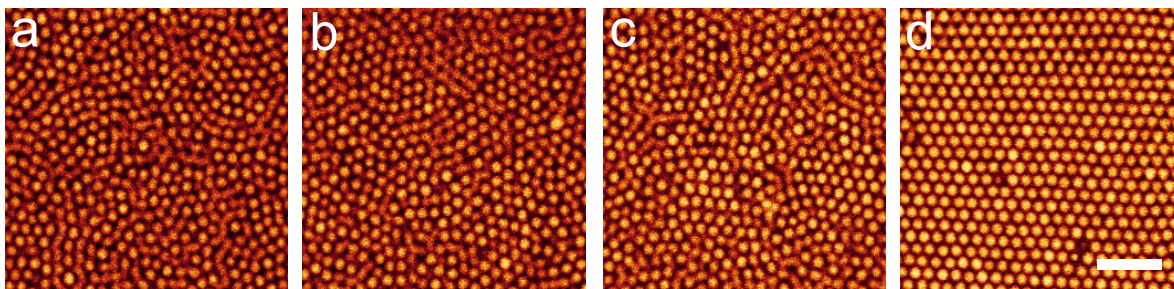


FIG. 6: (color online) Confocal microscopy images of crystallisation in nearly-hard spheres for $\phi = 0.54$. (a) 600 s ($2.3 \tau_\alpha$), (b) 4500 s ($17.4 \tau_\alpha$), (c) 7200 s ($27.9 \tau_\alpha$) (d) 81900 s ($316.9 \tau_\alpha$) bar=10 μm .

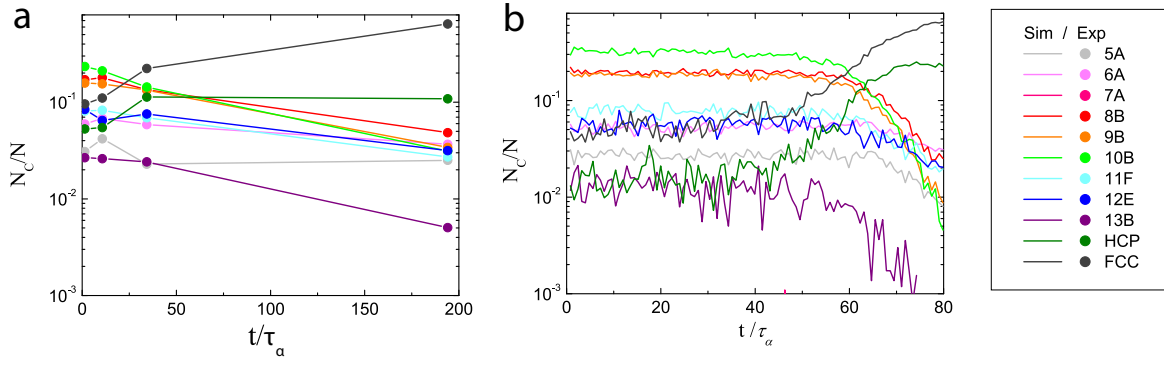


FIG. 7: (color online) Topological cluster classification analysis of crystallisation, experimental (a) and simulation data (b). Here $\phi = 0.56$.

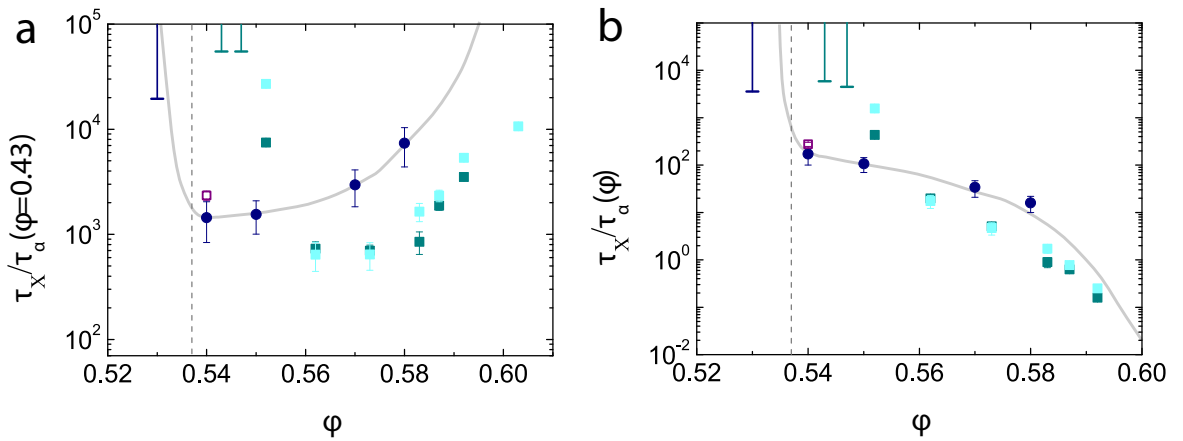


FIG. 8: (color online) Crystallisation times in terms of $\tau_\alpha(\phi = 0.43)$ (a) and $\tau_\alpha(\phi)$. Circles are experimental data, dark and light squares are simulation data for polydisperse systems of $N = 10976$ and $N = 2048$ respectively. Unfilled square is for a monodisperse system with $N = 10976$. Dashed lines are melting estimated as described in section II B. Solid lines are to guide the eye. Error bars extending upwards are lower bounds for crystallisation times determined from experiments (light lines) and simulations (dark lines) which did not crystallise.

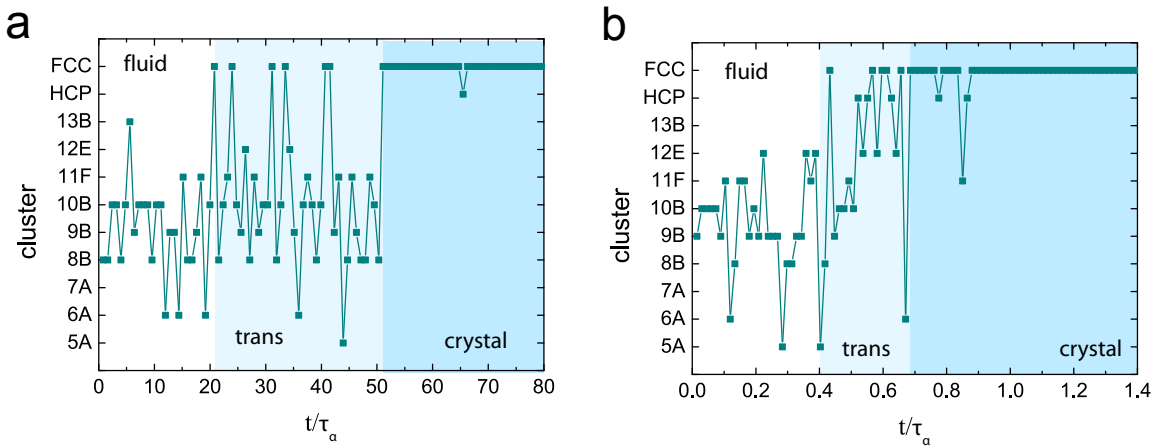


FIG. 9: (color online) History of a single particle. (a) $\phi = 0.55$, (b) $\phi = 0.58$. Shaded areas mark the different regimes of fluid, transition and crystal, as described in the text. Data are shown from Brownian dynamics simulations.

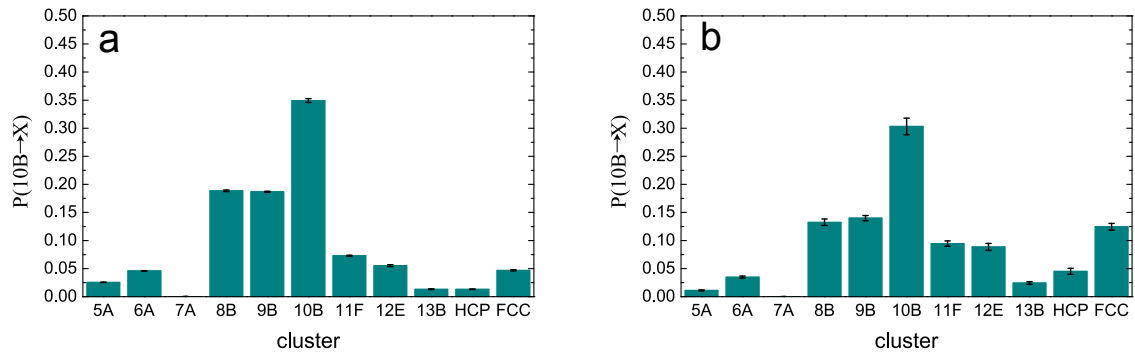


FIG. 10: (color online) Transitions from the 10B cluster. (a) $\phi = 0.55$, (b) $\phi = 0.57$. These are the probability for a particle to be found in a cluster at time $t + \tau_t$, given that it was in a 10B cluster at t . Here $\tau_t = 0.08\tau_\alpha$ for both (a) and (b). Data are shown from Brownian dynamics simulations.